Analytica Chimica Acta xxx (2016) 1–10

Contents lists available at ScienceDirect

Analytica Chimica Acta

journal homepage: www.elsevier.com/locate/aca

Controlled deposition of functionalized silica coated zinc oxide nano-assemblies at the air/water interface for blood cancer detection

Chandra Mouli Pandey [a, b, 1], Srishti Dewan [a, c, 1], Seema Chawla [c], Birendra Kumar Yadav [d], Gajjala Sumana [a, *], Bansi Dhar Malhotra [a, b, **]

[a] Biomedical Instrumentation Section, CSIR-National Physical Laboratory, New Delhi 110012, India
[b] Nanobioelectronics Laboratory, Department of Biotechnology, Delhi Technological University, Delhi 110042, India
[c] Biomedical Engineering Department, Deenbandhu Chhotu Ram University of Science & Technology, Haryana 131039, India
[d] Rajiv Gandhi Cancer Institute and Research Centre, Rohini, Delhi 110085, India

HIGHLIGHTS

- Stable and controlled deposition of Am-Si@ZnO nano-assemblies using LB technique.
- Uniform monolayer deposition of the Am-Si@ZnO LB film within the nanometer range.
- Am-Si@ZnO LB film shows enhanced electrochemical properties.
- Fabricated nucleic acid sensor is ultrasensitive (1×10^{-16} M) for CML detection.
- Validation with clinical samples of CML positive patients shows its potential for clinical diagnosis.

GRAPHICAL ABSTRACT

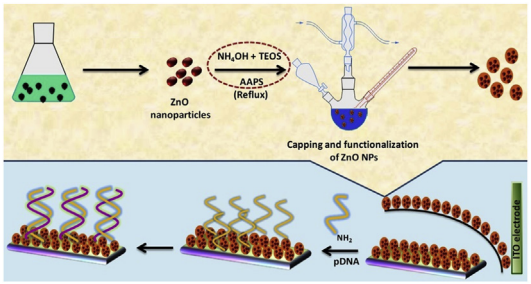

ARTICLE INFO

Article history:
Received 23 May 2016
Received in revised form
18 July 2016
Accepted 20 July 2016
Available online xxx

Keywords:
Langmuir-blodgett monolayer
Zinc oxide
Chronic myelogenous leukemia
Cancer
Nucleic acid biosensor

ABSTRACT

We report results of the studies relating to controlled deposition of the amino-functionalized silica-coated zinc oxide (Am-Si@ZnO) nano-assemblies onto an indium tin oxide (ITO) coated glass substrate using Langmuir-Blodgett (LB) technique. The monolayers have been deposited by transferring the spread solution of Am-Si@ZnO stearic acid prepared in chloroform at the air-water interface, at optimized pressure (16 mN/m), concentration (10 mg/ml) and temperature (23 °C). The high-resolution transmission electron microscopic studies of the Am-Si@ZnO nanocomposite reveal that the nanoparticles have a microscopic structure comprising of hexagonal assemblies of ZnO with typical dimensions of 30 nm. The surface morphology of the LB multilayer observed by scanning electron microscopy shows uniform surface of the Am-Si@ZnO film in the nanometer range (<80 nm). These electrodes have been utilized for chronic myelogenous leukemia (CML) detection by covalently immobilizing the amino-terminated oligonucleotide probe sequence *via* glutaraldehyde as a crosslinker. The response studies of these fabricated electrodes carried out using electrochemical impedance spectroscopy show that this Am-Si@ZnO LB film based nucleic acid sensor exhibits a linear response to complementary DNA (10^{-6}

* Corresponding author. Biomedical Instrumentation Section, CSIR-National Physical Laboratory, New Delhi 110012, India.
** Corresponding author. Nanobioelectronics Laboratory, Department of Biotechnology, Delhi Technological University, Delhi 110042, India.
E-mail addresses: sumanagajjala@gmail.com (G. Sumana), bansi.malhotra@gmail.com (B.D. Malhotra).
[1] These authors contributed equally to this work.

http://dx.doi.org/10.1016/j.aca.2016.07.024
0003-2670/

-10^{-16} M) with a detection limit of 1×10^{-16} M. This fabricated platform is validated with clinical samples of CML positive patients and the results demonstrate its immense potential for clinical diagnosis.

1. Introduction

Leukemia is a progressive disease wherein the bone marrow and other blood-forming organs produce increased numbers of abnormal leukocytes, leading to anemia and other manifestations [1]. Chronic myeloid leukemia (CML) is one of the most common type of leukemia, which is induced by the active breakpoint cluster region (BCR)/Abelson (ABL) oncogene [2]. The abnormality is produced by reciprocal translocation of chromosome 9 and 22 and it usually occurs in more than 95% of the CML patients [3,4]. The molecular analysis of this translocation shows that the breakpoints on chromosome 22 occur within 5.8 kilobases (kb) of the breakpoint cluster region (BCR) gene [3]. Thus, BCR/ABL is an important biomarker for early diagnosis of the disease, and for detection of minimal residual leukemia cells in the CML patients, especially after the bone marrow transplantation [5]. The conventional techniques like chromosome analysis, fluorescence *in situ* hybridization, flow cytometry, real-time quantitative reverse transcription polymerase chain reaction can be used for the BCR/ABL fusion gene detection [6]. However, some of the major drawbacks of these techniques include poor precision, cost and long delay etc. [7].

The electrochemical DNA biosensors based on nucleic acid hybridization have recently been explored for diagnosis of blood cancer [8–10]. DNA biosensors offer a new approach for rapid, sensitive, simple and low-cost detection of specific nucleic acid sequences [9,11]. Some electrochemical DNA sensors based on quantum dots (QD) and conducting polymers have been reported for detection of BCR/ABL oncogene [12,13]. It has been found that the immobilizing matrix plays an important role towards the fabrication of a biosensor [14,15]. In this context, an important issue for QD application in biosystems is the short/long-term toxicity of QDs [16]. Quantum dots are known to damage DNA and reduce the activity due to factors such as the surface coating [17]. Lin et al. fabricated an electro-chemical DNA biosensor based on glassy carbon electrode using methylene blue (MB) as the hybridization indicator [18]. This sensor shows the detection limit of 5.9×10^{-8} M. An impedance biosensor for detection of CML, based on DNA immobilized gold nanoparticles/gold modified electrode with a detection limit of 1.0×10^{-12} mol L^{-1} was fabricated by Ensafi et al. [19]. However, validation with the clinical patient samples was not reported. In spite of these developments, there is an urgent need for the availability of a sensitive, specific and mediator free reusable biosensor that can be used for early and reliable detection of CML.

The assembly of a modified material onto an electrode surface is crucial for the construction of an electrochemical biosensor as biomolecules are known to get denatured quickly due to physiological changes [20–22]. For the fabrication of a high-performance miniaturized biosensor, an important step is the deposition of ultra-thin ordered structures because the performance of the device depends strongly on the molecular arrangement [23,24]. In this regard, the composition of a monolayer based matrix has been found largely based on the Langmuir–Blodgett (LB) technique that involves the transfer of a monolayer, assembled at the gas–liquid interface to a solid substrate [25,26]. Recently, nanostructured oxides of metals like zinc, iron, titanium, have been found to play a significant role since they provide desired orientation to the biomolecules with negligible conformational changes [27–29]. Among the various metal oxides, zinc oxide nanoparticles (ZnONPs) due to their easy fabrication, biocompatibility, environmental friendly nature, and non-toxic synthesis route can be used for biosensor application [30–32]. Zinc oxide is a wide band gap semiconductor (Eg = 3.37 eV), which makes it more attractive for fabrication of high-efficiency nano-devices because of its high exciton binding energy of 60 meV and high mechanical and thermal stabilities [33,34].

We report results of studies relating to the fabrication of a novel electrochemical DNA sensor based on amino-functionalized silica coated ZnONPs (Am-Si@ZnO NPs) using LB technique. This platform has been utilized for the detection of BCR-ABL fusion gene of CML by covalently immobilizing probe sequence specific to CML. This optimized Am-Si@ZnO nano-assembly shows excellent specificity for single-base mismatch and complementary DNA after hybridization and the specific probe has been used for the assay of a PCR clinical sample of CML patient.

2. Material and methods

2.1. Chemicals

Zinc nitrate hexahydrate ($Zn(NO_3)_2 \cdot 6H_2O$), tetraethyl orthosilicate (TEOS, 98%), n-(2-aminoethyl)-3-aminopropyltrimethoxysilane (AAPS, 80%), lithium hydroxide ($LiOH \cdot H_2O$), glutaraldehyde were purchased from Sigma–Aldrich (USA). The other reagents were of analytical grade and were used as received. CML specific probe oligonucleotide sequence, complementary, non-complementary and one-base mismatch target sequence used in this work are procured from Sigma-Aldrich, USA and are as follows.

Probe DNA (pDNA): Amine–5′–TGT CCA CAG CAT TCC GCT GACC–3′
Complementary: 5′–GGT CAG CGG AAT GCT GTG GACA–3′
One-base mismatch: 5′–GCT CAG CGG AAT GCT GTG GACA–3′
Non-complementary: 5′–TAC TCG CAA TAA CGT GAT CTCC–3′

The reagents were prepared in deionized water (Millipore, 18.0 MΩ cm), and the solutions and glassware were autoclaved prior to use. Tris-E buffer (1 M Tris-HCl and 0.5 M EDTA, pH 8.0) was used to prepare all oligonucleotide solutions and stored at −20 °C.

2.2. Synthesis of zinc oxide nanoparticles

Zinc oxide nanoparticles (ZnONPs) were synthesized by a previously reported method with slight modifications [35,36]. The alkaline solution was prepared by dissolving $Zn(NO_3)_2 \cdot 6H_2O$ and LiOH of equal concentration (0.1 M) in water and ethylene glycol (5:1) [37]. The solution was kept for 6 h without stirring, and the temperature was maintained at 100 °C. After the hydrolysis reaction, the white precipitates thus formed were collected by centrifugation and thoroughly washed with deionized water (5 times) and dried in vacuum oven (60 °C) [35].

Please cite this article in press as: C.M. Pandey, et al., Controlled deposition of functionalized silica coated zinc oxide nano-assemblies at the air/water interface for blood cancer detection, Analytica Chimica Acta (2016), http://dx.doi.org/10.1016/j.aca.2016.07.024

2.3. Synthesis of silica-coated zinc oxide nanoparticles

Surface modification of ZnONPs with silica was carried out in two steps using modified sol-gel process [38,39]. Solution (A) was prepared by adding ethanol and water (7:3) in a round bottomed flask that was continuously stirred and maintained at pH 12.0 using NH_4OH. For the preparation of solution (B), TEOS (30 wt %) was added to the prepared ZnONPs, and the solution was ultrasonicated for 15–20 min (Fig. 1(A)) [40]. For modification of the surface, TEOS was contemplated, to render the surface more hydrophobic and make them compatible with other organic media [41]. This solution was thus injected into solution (A) with continuous stirring for 12 h at room temperature. The silica coated ZnONPs (Si@ZnONPs) were centrifuged and washed with ethanol (5–6 times), and dried overnight, in a vacuum oven at 80 °C.

2.4. Functionalization of Si@ZnO nanoparticles

The amino functionalization of the Si@ZnO NPs was carried out using APTES to render them suitable for covalent immobilization of biomolecules on the surface. Functionalization of Si@ZnO (500 mg) was carried out using 0.075 mmol of AAPS by overnight refluxing in toluene [40].

2.5. Langmuir-Blodgett film preparation

Prior to deposition, ITO was hydrolyzed by immersing in the $H_2O_2/NH_4OH/H_2O$ solution (1:1:5, v/v) for about 30 min at 80 °C. The Langmuir trough was used for the preparation of Langmuir films of Am-Si@ZnO nanoparticles on hydrolyzed ITO glass (2 mm × 1 mm). Freshly prepared solution of Am-Si@ZnO NPs was diluted in chloroform (10 mg/ml) with stearic acid (1 mg/ml) in the ratio of 2:1, respectively and ultrasonicated for 30 min just before spreading (Fig. 1(B)). An optimized amount (30 μl) of the prepared material was spread at the water/air interface of the trough. After 15 min (chloroform evaporation), the particles were compressed with a barrier speed of 30 cm^2/s to record the surface area isotherm. The value of pressure at which quasi-solid behavior of monolayer appeared was found to be 16 mN/m at 23 °C. At this optimized pressure and temperature, the monolayers (2, 3 and 6) were transferred by vertical deposition, with interval of 300 s and 60 s for top and bottom dipper position, respectively.

2.6. Immobilization of probe DNA and hybridization

Glutaraldehyde was used as a cross-linker for bioconjugation of aminated pDNA to the Am-Si@ZnO/ITO electrode surface. For this purpose, the Am-Si@ZnO/ITO surface was activated by incubation in aqueous glutaraldehyde solution (0.1% v/v) for 1 h followed by washing with deionized water [42]. For coupling between the amine terminal of pDNA and the glutaraldehyde-modified Am-Si@ZnO/ITO electrode, 20 μL of pDNA was spread onto the modified electrode surface and kept in a humid chamber at room temperature (25 °C) for 4 h. The pDNA/Am-Si@ZnO/ITO bioelectrode was then rinsed with Tris–HCl (10 mM) and EDTA (1 mM) buffer solution (TE, pH 8.0) to remove any physically adsorbed pDNA on the electrode surface. This bioelectrode was further used for detection of CML by hybridizing various concentrations (10^{-6}-10^{-16}) of complementary target DNA.

2.7. Instruments

Monolayers deposition was done in an LB trough (NIMA 601A). Ultraviolet–visible (UV-Vis) absorption studies were carried out on UV-Vis spectrophotometer (Phoenix 2200DPCV). Fourier transform infrared (FTIR) measurements were employed in attenuated total reflection (ATR) mode, with germanium waveguide, on a Perkin–Elmer Spectrum BX II spectrophotometer. The FTIR signal was obtained by averaging 64 scans at the resolution of 4 cm^{-1}. Contact angle (CA) measurements were taken on a contact angle meter

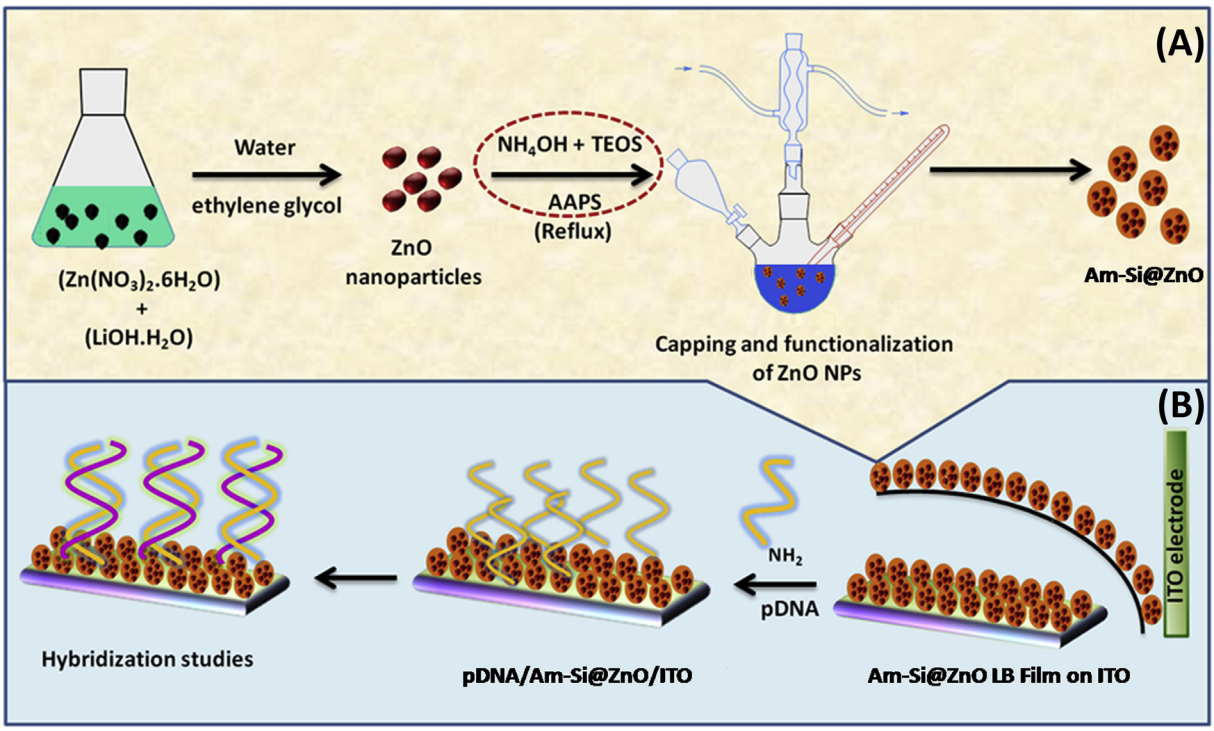

Fig. 1. Schematic illustration for the (A) synthesis of Am-Si@ZnO and (B) LB deposition Am-Si@ZnO on ITO electrode and subsequent DNA sensor fabrication.

Please cite this article in press as: C.M. Pandey, et al., Controlled deposition of functionalized silica coated zinc oxide nano-assemblies at the air/water interface for blood cancer detection, Analytica Chimica Acta (2016), http://dx.doi.org/10.1016/j.aca.2016.07.024

(Data Physics OCA15EC). The morphological characterization was carried out on a field emission transmission electron microscope (TEM; JEOL JEM-2100F) at an accelerating voltage of 200 keV and on a scanning electron microscope (SEM, LEO 440). Electrochemical characterization was conducted on an Autolab potentiostat/galvanostat (Eco Chemie, Netherlands) using a three-electrode system with ITO as the working electrode, Ag/AgCl as a reference electrode, and platinum foil as a counter electrode, in phosphate-buffer saline (PBS 100 mM, pH 7.4, and 0.9% NaCl).

3. Results and discussion

3.1. Characterization

The results of X-ray diffraction studies conducted on ZnO NPs show presence of the sharp peaks at $2\theta = 36.25°$ (101), 31.77° (100), 34.42° (002), 56.60° (110), 62.86° (103), indicating polycrystalline structure (JCPDS 36-1451), having hexagonal shape with lattice constants $a = b = 0.32$ nm and $c = 0.52$ nm (Fig. S1). No other characteristic peaks of any impurities were observed, suggesting that high-quality ZnONPs were synthesized. The crystalline size of the synthesized ZnONPs was found to be 10.25 nm using the Debye-Scherrer formula. Further, the UV–Vis absorption specta of ZnO nanoparticles shows an excitonic absorption peak at about 290 nm (Fig. S2(A)), that lies much below the band gap wavelength of 388 nm of bulk ZnO. The peak at ~290 nm in the spectra is due to the interband transition of the copper electrons from a deep level of valence band [36]. The blue shift in the peak centered at ~290 nm in absorption spectra is ascribed to the transition of electrons from the most inner shell of copper to the uppermost shell as the time passes. This behavior is typically shown by many semiconductors which arise due to internal electric fields within the crystal and inelastic scattering of the charge carriers by photons [36]. In case of the Am-Si@ZnO NPs, a peak is observed around ~375 nm (Fig. S2(B)) shows a red shift, in the peaks.

3.2. Zeta potential studies

The size distribution profile of the aqueous suspension of ZnONPs exhibits a particle size of around 15 nm determined via dynamic light scattering technique (Fig. S3(A)). On coating, the ZnONPs with silica the average particle size increased to 60 nm due to coating of the ZnONPs by silica (Fig. S3(B)). The total surface charge of the synthesized ZnONPs was determined using the Smoluchowski method, and the results are shown in Fig. S3. The ZnONPs exhibit a zeta potential value of 10 mV (Fig. S3(C)). After encapsulation with SiO_2 the zeta potential was found to be −34 mV (Fig. S3(D)). To investigate the effect of APTES functionalization on the Si@ZnO, the surface charge of the nanoparticles was measured, and an increase in the zeta potential from −34 mV to −25 mV was observed indicating presence of the positively charged $-NH_2$ groups. This is indirect evidence showing that the amino group is perhaps conjugated to the Si@ZnO NPs, due to hydrolysis between the APTES and TEOS.

3.3. Microscopic analysis of the nanocomposite ZnONPs and Si@ZnO NPs

The TEM images of the ZnONPs and Si@ZnO NPs are shown in Fig. 2. It appears that ZnONPs are polydispersed in size and that the nanoparticles are spherical or hexagonal in shape (Fig. 2(A)). The diameter of the ZnONPs is in the range of 10–15 nm which is in agreement with the apparent crystallite size determined by XRD. Fig. 2(B) shows hexagonal morphology of the ZnONPs while Fig. 2(C) shows high-resolution TEM image of a hexagonal ZnO in the same sample and the lattice image shows (002) plane of ZnO with d-spacing value as expected for perfect crystalline ZnO. The TEM image of bare silica shows the size of the particle to be as 50 nm (Fig. 2(D)). After surface modification, spherical aggregates of silica coating on hexagonal ZnONPs were observed with size of 70–80 nm (Fig. 2(E)). The HRTEM images of Si@ZnO are shown in Fig. 2(F), which clearly shows wrapping of the ZnO with SiO_2.

3.4. Surface measurements of Am-Si@ZnO Langmuir monolayer

The pressure area isotherms of Am-Si@ZnO Langmuir monolayer on air-water subphase were recorded at different temperatures with varying ratio of the material with respect to stearic acid. Stearic acid acted as a spacer between the particles, as it reduced the aggregate formation and improved the spreading behavior of monolayer on the surface [43]. At 23 °C an optimized quantity (30 μl) of prepared solution with stearic acid (in 2:1 ratio), the area-pressure curve (Fig. 3(A)) showed a sharp kick. The pressure at which material showed the quasi-solid behavior of monolayer was found to be 16 mN/m and the collapsing pressure was found to be 38 mN/m. The observed mean molecular area of the surface was determined to be 2315 $Å^2$/particle, when the surface pressure was set at 0 mN/m.

3.5. Transfer characteristics of Am-Si@ZnO Langmuir monolayers

Langmuir monolayers of Am-Si@ZnO nanoparticles were transferred on hydrolyzed ITO substrate with surface pressure of 16 mN/m at 23 °C. The hydrophobic substrate was positioned perpendicular to the air-water interface, and the monolayers were subsequently deposited by vertical dipping at a rate of 10 mm min^{-1} to obtain Y-type multilayer film (6 layers) shown in Fig. 3(B). The single monolayer of Am-Si@ZnO was transferred onto the hydrophobic substrate in each upward and downward stroke. Transfer onto the substrate as estimated from the change in surface area at the air-water interface, was nearly the same for each monolayer and the results of kinetic measurements as a function of time reveals that it took 30 min for stable monolayers formation (Fig. 3(C)).

3.6. FTIR studies

FT-IR spectra of the bare ZnONPs shows a prominent peak at ~453 cm^{-1} (Fig S4 (i)), due to the stretching vibration of Zn–O bond. While the peaks observed at 1550–1700 cm^{-1} and 3100–3600 cm^{-1} can be attributed to the hydroxyl groups [44]. The Si–O–Si asymmetric stretching vibration band of 980–1190 cm^{-1} is found only in the Am-Si@ZnO NPs spectrum (Fig S4 (ii)), compared to the bare ZnONPs. In Am-Si@ZnO NPs, N–H stretch and hydroxyl group at 3300-3400 cm^{-1} and 3250-3330 cm^{-1} respectively are observed, indicating presence of the primary amine in nanocomposite [40,45].

3.7. Morphological characterization of the electrode and bioelectrode

The morphological studies of the different layers of Am-Si@ZnO LB film on the ITO electrode were studied using SEM. The SEM image of four layers of Am-Si@ZnO nanoparticles (Fig. 4(A)) shows that particles are far apart whereas in the six layers (Fig. 4(B)) the particle distribution is denser (Fig. 4(C)). After immobilization of pDNA on the 6 layered Am-Si@ZnO/ITO electrode globular structures appeared onto the Am-Si@ZnO LB film confirming the attachment of DNA onto the Am-Si@ZnO LB film (Fig. 4(D)). Further, experiments were carried out by directly depositing the Am-

Please cite this article in press as: C.M. Pandey, et al., Controlled deposition of functionalized silica coated zinc oxide nano-assemblies at the air/water interface for blood cancer detection, Analytica Chimica Acta (2016), http://dx.doi.org/10.1016/j.aca.2016.07.024

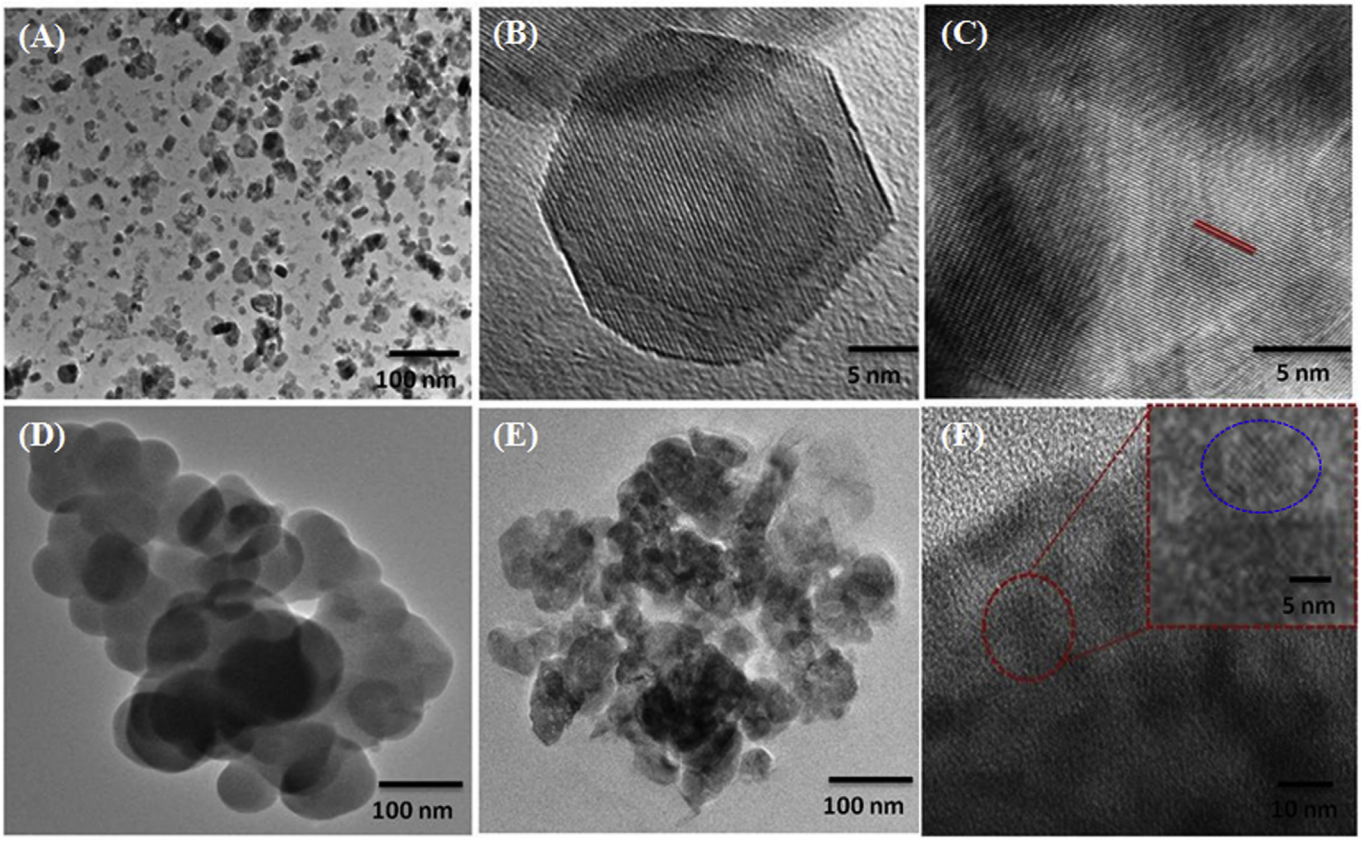

Fig. 2. (A) TEM image of ZnO NPs (B) Magnified image showing hexagonal structure of ZnONPs (C) HRTEM image of ZnONPs (D) TEM image of Silica NPs (E) TEM image of Si@ZnO NPs (F) HRTEM image of Si@ZnO NPs.

Si@ZnO onto ITO coated glass substrate (Fig. 4(E)). It was observed that aggregation of the nanocomposite occurred on the electrode that upon immobilization of pDNA showed an uneven distribution of the pDNA (Fig. 4(F)).

3.8. Electrochemical characterization

3.8.1. Electrochemical studies of the monolayers

Electrochemical impedance spectroscopic (EIS) studies were conducted to evaluate the electrical properties of the multilayer assembly to provide the information during the step deposition of the Am-Si@ZnO LB layers. Impedance spectra were recorded after deposition of each layer of Am-Si@ZnO LB film to investigate the effect of the structure and thickness of the multilayer on the overall interfacial properties. The impedance spectra seen in the Nyquist plot consists of a semicircle portion observed at higher frequencies indicating electron transfer process, whereas the linear part at low frequencies corresponds to the diffusion controlled process [11]. The modified Randles equivalent circuit (inset Fig. 5(B)) was employed to fit the impedance spectra of the fabricated biosensor. The circuit consists of the electrolyte resistance (Rs) between the working and the reference electrode, the Warburg impedance (Z_W), associated with the diffusion process of redox probe ions from the bulk solution to the electrode–solution interface, the electron transfer resistance (Rct) and the constant phase element CPE (related to the double layer capacitance) [24]. The impedance measurements were carried out at the open circuit voltage. The tested frequency range was from 1 Hz to 100 kHz with an amplitude of ±5 mV. With increase in the number of layers of Am-Si@ZnO from two to six, the R_{CT} value decreases (Fig. 5(A)) correspondingly. Changes can be clearly seen in the spectra during the stepwise formation of the multilayer assemblies (2 layers (curve iii), 4 layers (curve ii) and 6 layers (curve i)). The diameter of the semicircle decreases with an increasing number of Am-Si@ZnO LB film, which is due to increase in the film thickness and change in the apparent charge transfer resistance. The interfacial properties of the electrode after each different monolayer (2, 4, 6 layers) were investigated as shown in Table 1. It was found that with increase in the number of Am-Si@ZnO monolayer there was an increase in the exchange current per unit geometric area and the apparent electron transfer rate constant (K_{app}) and it was maximum for 6 layers. To avoid any non-specific adsorption of the cDNA, the optimization of the pDNA on the Am-Si@ZnO/ITO electrode was conducted by varying the pDNA concentration from 10^{-5} M to 10^{-10} M. As shown in Fig. S5, the R_{CT} value leveled off at 10^{-6} M pDNA concentration suggesting that maximum immobilization was achieved at this concentration.

Cyclic voltammetry studies were performed, using a three-electrode system in PBS solution (100 mM, pH 7.0, 150 mM NaCl) containing 5 mM $[Fe(CN)6]^{-3/-4}$. The results of cyclic voltammetric studies, obtained as a function of scan rate (υ, 10–300 mV s^{-1}), for Am-Si@ZnO/ITO electrode and pDNA/Am-Si@ZnO/ITO bioelectrode are shown in Figs. S6(A) and (B), respectively. The observed positive and negative peaks correspond to the oxidation and reduction reactions of the $[Fe(CN)_6]^{-3/-4}$ redox pair, respectively. The peak currents (*I*p) for both oxidation and reduction follow a linear relation with respect to square root of the scan rate (inset (i), Fig. S6(A), (B)) indicating the existence of diffusion-controlled electrochemical reaction rates for the redox pair at the electrode. It was observed that the oxidation peak shifted to a more positive value

Please cite this article in press as: C.M. Pandey, et al., Controlled deposition of functionalized silica coated zinc oxide nano-assemblies at the air/water interface for blood cancer detection, Analytica Chimica Acta (2016), http://dx.doi.org/10.1016/j.aca.2016.07.024

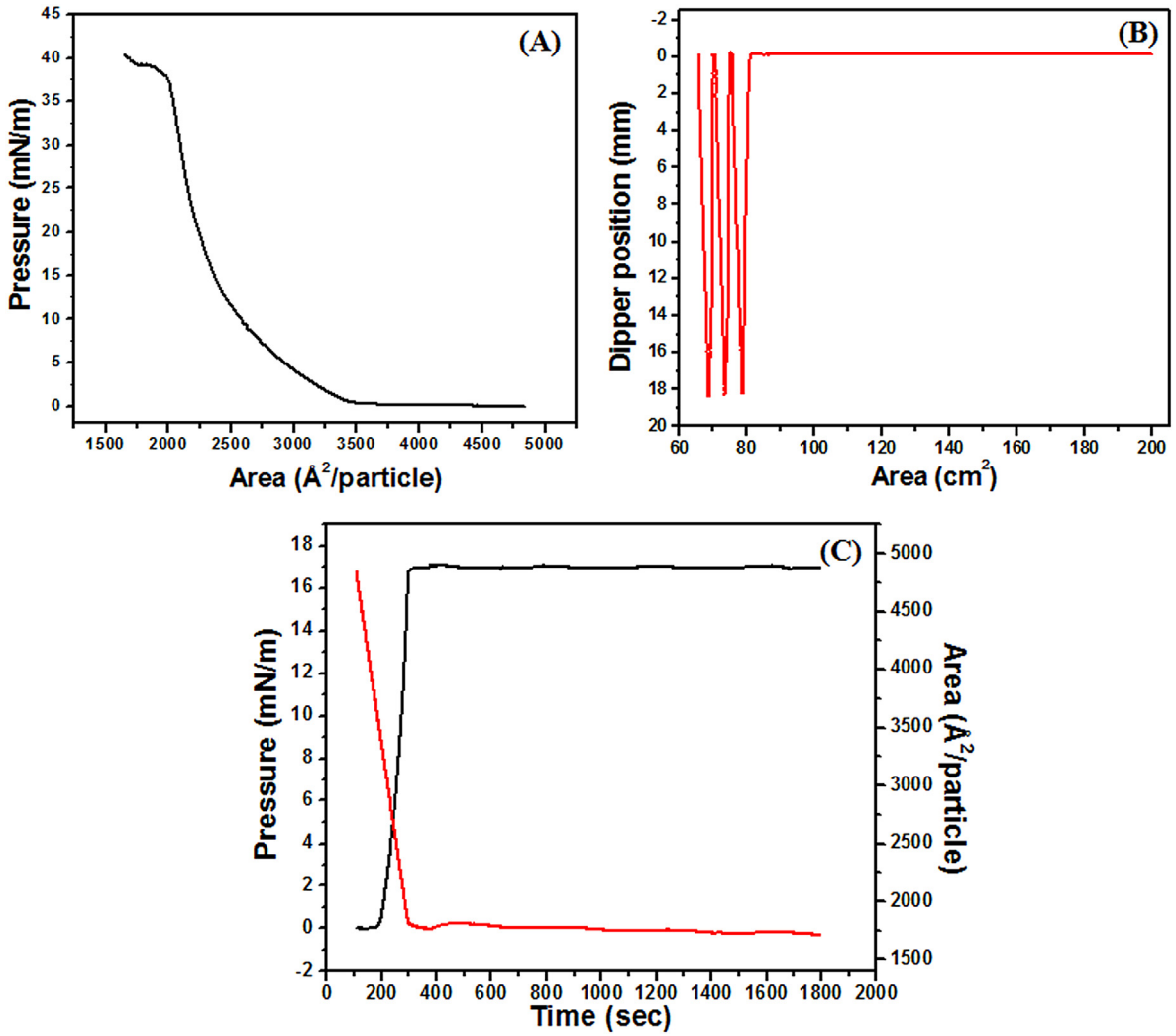

Fig. 3. (A) Surface pressure–area isotherm of Am-Si@ZnO NPs (B) Deposition curve of Am-Si@ZnO NPs on ITO substrate (C) Kinetic measurements showing variation in the particulate surface area at the air–water interface as a function of time at a constant surface pressure.

and the reduction peak to more negative values where both the peak potentials were linearly dependent on the log of the scan rate (inset (ii), Fig. S6(A), (B)). Using Laviron's equations, the value of electron transfer coefficient (α), for n number of electrons, was determined from the slope of two straight lines with anodic and cathodic slopes of $2.303RT/(1-\alpha)nF$ and $-2.303RT/\alpha nF$, respectively [42]. The diffusion coefficient (D) was determined by a concentration gradient of $[Fe(CN)_6]^{3-/4-}$ ions between bulk and interface and was calculated via the Randles–Sevick equation (1):

$$Ip = \left(2.69 \times 10^5\right)\alpha^{1/2} n^{3/2} \mathrm{ACD}^{1/2} \upsilon^{1/2} \quad (1)$$

where C is the molar concentration of $[Fe(CN)_6]^{3-/4-}$, and A is the electrode surface area that is immersed in the electrolyte solution (0.5 cm^2). The D value for Am-Si@ZnO/ITO electrode was found to be greater than that of the pDNA/Am-Si@ZnO/ITO electrode. By using the calculated diffusion coefficient, the electroactive surface area (A_e) for the Am-Si@ZnO/ITO electrode and pDNA/Am-Si@ZnO/ITO electrode was calculated to be 1.1685 mm^2 and 0.9239 mm^2, respectively (Table 2) [42].

3.8.2. Electrochemical response studies

For the electrochemical response studies, 6 layers of Am-Si@ZnO LB film were used. When pDNA was immobilized onto the Am-Si@ZnO/ITO electrode, an increase in R_{CT} value was observed due to the negatively charged phosphate backbone of pDNA exposed to the electrolyte, which in turn perhaps repelled $[Fe(CN)_6]^{-3/-4}$ (Fig. 5(B); curve ii). When the pDNA was incubated with its complementary target DNA sequence (cDNA), the hybridization reaction occured and more negatively charged phosphate backbones were introduced. Hence, the R_{CT} value increased following the formation of double-stranded DNA (Fig. 5(B); curve iii). Thus with a change in negative charge and conformation transition, there was a change in the interfacial properties. The difference between the value of R_{CT} for the pDNA immobilized electrode and after hybridization with cDNA ($\Delta R_{CT} = R_{CT}$cDNA- R_{CT}pDNA) was used as the measurement signal. The analytical signal (in terms of ΔR_{CT}) showed a linear relationship with the logarithmic value of the complementary target DNA concentration ranging from 10^{-16} to 10^{-6} M (Fig. 5(D); curve (i)) and follows the following equation:

$$\Delta R_{CT} = 1840.18 + 105.26[\log(\text{concentration of cDNA})] \quad (2)$$

with a linear regression coefficient of 0.9960. The detection limit was calculated using the expression, 3σ/sensitivity, where σ is the standard deviation of the blank electrode. The detection limit for

Please cite this article in press as: C.M. Pandey, et al., Controlled deposition of functionalized silica coated zinc oxide nano-assemblies at the air/water interface for blood cancer detection, Analytica Chimica Acta (2016), http://dx.doi.org/10.1016/j.aca.2016.07.024

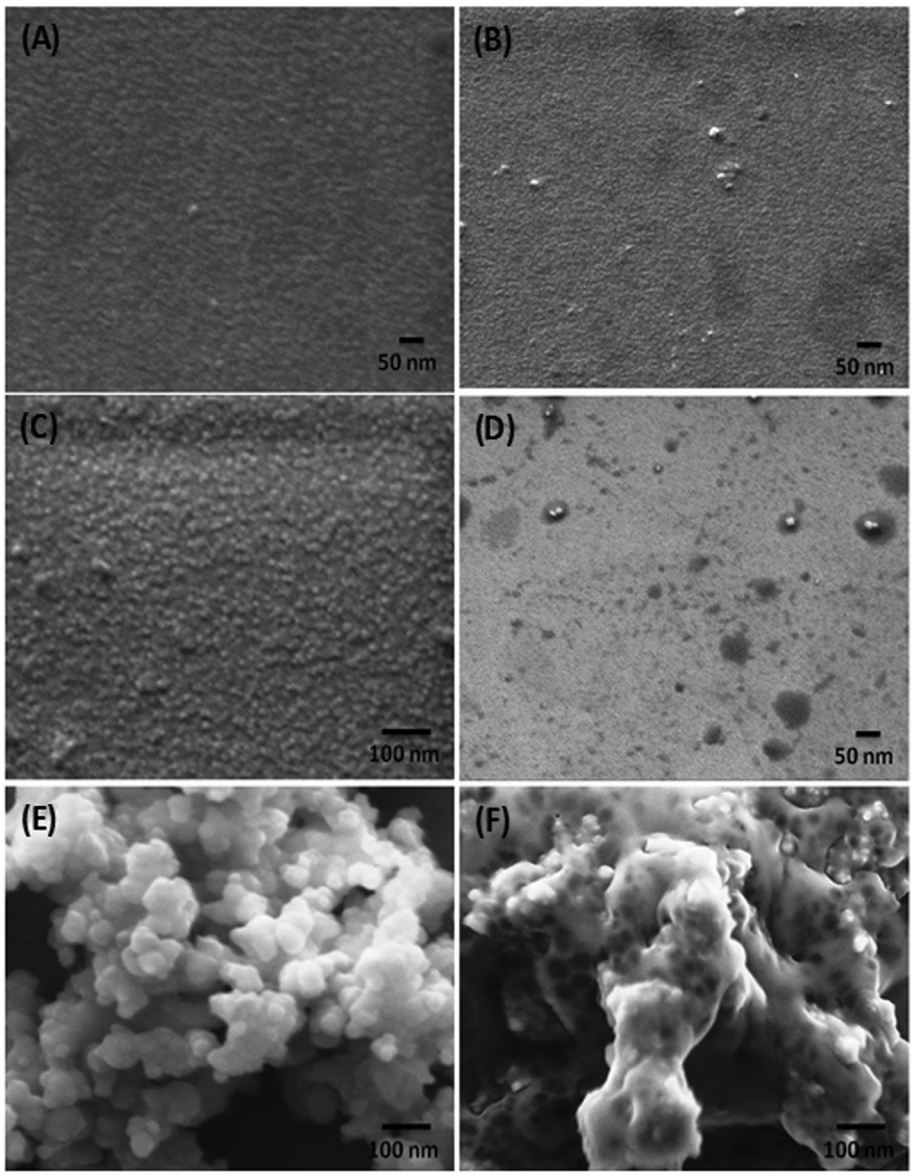

Fig. 4. SEM image of (A) 4 layered LB film of Am-Si@ZnO/ITO, (B) 6 layered LB film of Am-Si@ZnO/ITO. (C) Magnified SEM image of 6 layered LB film of Am-Si@ZnO/ITO. SEM image of (D) pDNA immobilized on 6 layered LB film of Am-Si@ZnO/ITO; (E) Self assembled layers of Am-Si@ZnO on ITO substrate (F) pDNA immobilization on Am-Si@ZnO/ITO (self assembled).

pDNA/Am-Si@ZnO/ITO electrode was found to be 1×10^{-16} M, which is quite higher in comparison to pDNA/ZnO/ITO electrode (1×10^{-13} M, Fig. 5(D); curve (ii)). The enhanced sensitivity is probably due to the favourable orientation of the pDNA onto Am-Si@ZnO LB films. The reproducibility of the fabricated pDNA/Am-Si@ZnO/ITO electrode was investigated by using the interassays coefficient of variation, which was evaluated by analysis of the same concentration of cDNA (10^{-16} M and 10^{-12} M) using five equally prepared electrodes [46]. Five independently made genosensor exhibited similar R_{CT} response and the interassay variation coefficient of interassays was 5.1% (10^{-16} M) and 4.4% (10^{-12} M). The low relative standard deviation indicates that the proposed Am-Si@ZnO LB film based nucleic acid sensor has good repeatability. Further, Langmuir isotherm approach was used to determine the association constant (K_a) for binding interaction assuming equal binding energy for all binding sites [47]. The K_a was estimated from the slope of the regression equation and found to be 0.584 M [46,47]. The fabricated pDNA/Am-Si@ZnO/ITO bioelectrode showed enhanced sensitivity and linearity range as compared to other biosensors reported for CML detection (Table ST1).

3.8.3. *Specificity studies of the bioelectrode*

The specificity of the pDNA/Am-Si@ZnO/ITO bioelectrode towards different target DNA sequences (complementary, non-complementary and one base mismatch) was studied using EIS (Fig. S7). On incubation of the bioelectrode with non-complementary DNA (Fig. S7, curve ii), there was a slight or negligible change in the Rct value with respect to the pDNA (curve i). Since the non-complementary DNA bases do not match with the pDNA bases it is expected that there is no hybridization taking place and hence the Rct should result in a semicircle diameter similar to that of pDNA/Am-Si@ZnO/ITO bioelectrode. When the pDNA/Am-Si@ZnO/ITO bioelectrode was immobilized with one-base mismatch DNA sequence, there was a slight increase in semicircle

Please cite this article in press as: C.M. Pandey, et al., Controlled deposition of functionalized silica coated zinc oxide nano-assemblies at the air/water interface for blood cancer detection, Analytica Chimica Acta (2016), http://dx.doi.org/10.1016/j.aca.2016.07.024

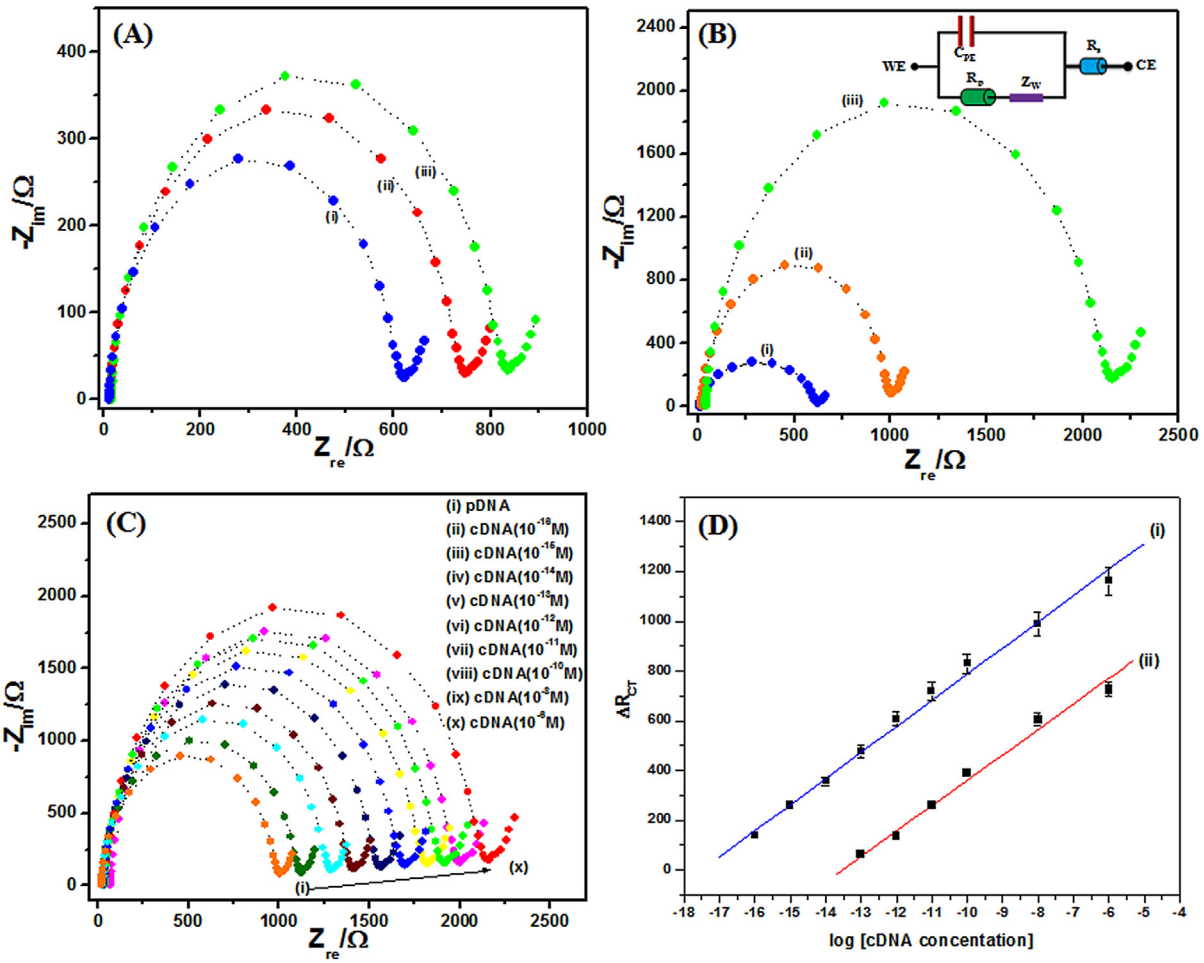

Fig. 5. (A) Nyquist diagram (Z_{im} versus Z_{re}) for the Faradic impedance of (i) 6, (ii) 4, (iii) 2 LB layers of Am-Si@ZnO/ITO. (B) Nyquist diagram (Z_{im} versus Z_{re}) for the Faradic impedance of (i) 6 layers of Am-Si@ZnO/ITO, (ii) pDNA/Am-Si@ZnO/ITO (iii) cDNA/pDNA/Am-Si@ZnO/ITO. (C) Nyquist diagram (Z_{im} versus Z_{re}) for the Faradic impedance of cDNA (10^{-6} M – 10^{-16} M) on pDNA/Am-Si@ZnO/ITO. (D) Linearity relation curve between ΔR_{CT} and log of concentrations of cDNA for (i) pDNA/Am-Si@ZnO/ITO electrode and, (ii) pDNA/ZnO/ITO electrode.

Table 1
Kinetic parameters calculated for the different Am-Si@ZnO LB layers deposited on ITO electrode using EIS.

No. of Layers	R_{CT} (Ω)	K_{app} (cm/s)	I_o (A/cm^2)
6 layers	606.880	1.75×10^{-7}	4.23×10^{-5}
4 layers	731.853	1.45×10^{-7}	3.51×10^{-5}
2 layers	819.643	1.29×10^{-7}	3.13×10^{-5}
pDNA	986.864	1.07×10^{-7}	2.604×10^{-5}

diameter in comparison to that of the pDNA/Am-Si@ZnO/ITO bioelectrode (curve iii). This explains partial hybridization of pDNA with the complementary bases of the one-base mis-match DNA resulting in increased negative charge of the electrode surface which repelled the marker ion [42]. These results reveal selectivity of the pDNA/Am-Si@ZnO/ITO bioelectrode towards different target DNA sequences. The negligible change in the value of R_{CT} was observed when pDNA/Am-Si@ZnO/ITO bioelectrode was treated with non-complementary DNA and one-base mismatch, which shows that fabricated bioelectrode is highly specific for CML detection.

3.9. Validation of the biosensor with patient samples

To test real application of the fabricated DNA biosensor, positive real samples of CML patient, were procured from Rajiv Gandhi Cancer Institute and Research Centre, Delhi, India after PCR amplification. Prior to performing the electrochemical assay with PCR amplicons of BCR-ABL fusion gene, the samples were ultrasonicated to allow shearing. Gel electrophoresis experiment of the

Table 2
Kinetic parameter calculated for the Am-Si@ZnO/ITO electrode and pDNA/Am-Si@ZnO/ITO electrode.

Name of electrode	Electron transfer coefficient (α)	Charge transfer rate constant (ks; s^{-1})	Diffusion coefficient (D; cm^2s^{-1})	Electroactive surface area (A; mm^2)	Average surface concentration (Γ; mol cm^2)
Am-Si@ZnO/ITO	0.596	0.0121	3.08×10^{-11}	1.1685	3.55×10^{-8}
pDNA/Am-Si@ZnO/ITO	0.5158	0.0738	1.89×10^{-11}	0.9239	2.56×10^{-8}

Please cite this article in press as: C.M. Pandey, et al., Controlled deposition of functionalized silica coated zinc oxide nano-assemblies at the air/water interface for blood cancer detection, Analytica Chimica Acta (2016), http://dx.doi.org/10.1016/j.aca.2016.07.024

fragmented cDNA samples was performed to obtain an estimation of fragments length with respect to the sonication time (Fig. S7). It was revealed that fragmentation in the length range of about 50 bases occurred after 15 min of sonication (Fig. S7; panel iii). The R_{CT} value of the positive real sample gave a mean average of 2.3 KΩ and 2.45 KΩ (Fig. S8; curve v and vi), which were similar to that of the cDNA (curve iv). The analysis of EIS results shows that the fabricated nucleic acid sensor performed equally well despite the fact that BCR-ABL from real sample is much longer than that of the synthetic target DNA [48].

4. Conclusions

An impedimetric nucleic acid sensor based on covalently immobilized CML specific DNA onto Am-Si@ZnO LB films has been developed. The sensing results carried out using EIS studies reveal that the pDNA/Am-Si@ZnO/ITO nucleic acid sensor shows linear range, 10^{-16} M-10^{-6} M with an increased sensitivity of 10^{-16} M for CML detection. This LB based nucleic acid sensor has been successfully used to distinguish CML positive patient samples. Efforts are being made to integrate the Am-Si@ZnO LB film with the microfluidic techniques to execute on-chip electrochemical DNA sensor in a single platform. Thus this platform holds great promise for development of ultrasensitive bioassay for cancer monitoring.

Acknowledgement

We thank Director, CSIR-NPL, New Delhi, India for his interest and support in this work. We thank Dr. R.K.Kotnala (CSIR-NPL) for interesting discussions. C.M. Pandey acknowledges the financial support received from Department of Science and Technology, India under DST-INSPIRE Faculty project (Grant No. DST/INSPIRE/04/2015/000932).

Appendix A. Supplementary data

Supplementary data related to this article can be found at http://dx.doi.org/10.1016/j.aca.2016.07.024.

References

[1] A.A. Ensafi, M. Taei, H.R. Rahmani, T. Khayamian, Sensitive DNA impedance biosensor for detection of cancer, chronic lymphocytic leukemia, based on gold nanoparticles/gold modified electrode, Electrochim. Acta 56 (2011) 8176–8183.
[2] M.W.N. Deininger, J.M. Goldman, J.V. Melo, The molecular biology of chronic myeloid leukemia, Blood 96 (2000) 3343–3356.
[3] F. Morel, C. Ka, M.J. Le Bris, A. Herry, P. Morice, P. Bourquard, J.F. Abgrall, C. Berthou, M. De Braekeleer, Deletion of the 5[prime] abl region in Philadelphia chromosome-positive chronic myeloid leukemia, Leukemia 17 (2003) 473–474.
[4] J.P. Radich, T. Gooley, E. Bryant, T. Chauncey, R. Clift, L. Beppu, S. Edmands, M.E.D. Flowers, K. Kerkof, R. Nelson, F.R. Appelbaum, The significance of bcr-abl molecular detection in chronic myeloid leukemia patients "late," 18 months or more after transplantation, Blood 98 (2001) 1701–1707.
[5] S. Slavin, A. Nagler, E. Naparstek, Y. Kapelushnik, M. Aker, G. Cividalli, G. Varadi, M. Kirschbaum, A. Ackerstein, S. Samuel, A. Amar, C. Brautbar, O. Ben-Tal, A. Eldor, R. Or, Nonmyeloablative stem cell transplantation and cell therapy as an alternative to conventional bone marrow transplantation with lethal cytoreduction for the treatment of malignant and nonmalignant hematologic diseases, Blood 91 (1998) 756–763.
[6] M.A. Tainsky, Genomic and proteomic biomarkers for Cancer: a multitude of opportunities, Biochim. Biophys. Acta 1796 (2009) 176–193.
[7] R.W. McKenna, Multifaceted approach to the diagnosis and classification of acute leukemias, Clin. Chem. 46 (2000) 1252–1259.
[8] K.J. Odenthal, J.J. Gooding, An introduction to electrochemical DNAbiosensors, Analyst 132 (2007) 603–610.
[9] T.G. Drummond, M.G. Hill, J.K. Barton, Electrochemical DNA sensors, Nat. Biotech. 21 (2003) 1192–1199.
[10] X. Chen, L. Wang, S. Sheng, T. Wang, J. Yang, G. Xie, W. Feng, Coupling a universal DNA circuit with graphene sheets/polyaniline/AuNPs nanocomposites for the detection of BCR/ABL fusion gene, Anal. Chim. Acta 889 (2015) 90–97.
[11] C.M. Pandey, G. Sumana, B.D. Malhotra, Microstructured cystine dendrites-based impedimetric sensor for nucleic acid detection, Biomacromolecules 12 (2011) 2925–2932.
[12] L. Wang, E. Hua, M. Liang, C. Ma, Z. Liu, S. Sheng, M. Liu, G. Xie, W. Feng, Graphene sheets, polyaniline and AuNPs based DNA sensor for electrochemical determination of BCR/ABL fusion gene with functional hairpin probe, Biosens. Bioelectron. 51 (2014) 201–207.
[13] W. Zhang, Electrochemically reduced graphene oxide supported poly(indole-5-carboxylic acid) nanocomposite for genosensing application, RSC Adv. 5 (2015) 103649–103655.
[14] P.R. Solanki, A. Kaushik, V.V. Agrawal, B.D. Malhotra, Nanostructured metal oxide-based biosensors, NPG Asia Mater 3 (2011) 17–24.
[15] A. Sharma, C.M. Pandey, Z. Matharu, U. Soni, S. Sapra, G. Sumana, M.K. Pandey, T. Chatterjee, B.D. Malhotra, Nanopatterned cadmium selenide Langmuir–-blodgett platform for leukemia detection, Anal. Chem. 84 (2012) 3082–3089.
[16] J. Drbohlavova, V. Adam, R. Kizek, J. Hubalek, Quantum dots-characterization, preparation and usage in biological systems, Int. J. Mol. Sci. 10 (2009) 656–673.
[17] M.A. Walling, J.A. Novak, J.R.E. Shepard, Quantum dots for live cell and in vivo imaging, Int. J. Mol. Sci. 10 (2009) 441–491.
[18] X.-H. Lin, P. Wu, W. Chen, Y.-F. Zhang, X.-H. Xia, Electrochemical DNA biosensor for the detection of short DNA species of Chronic Myelogenous Leukemia by using methylene blue, Talanta 72 (2007) 468–471.
[19] A.A. Ensafi, H. Karimi-Maleh, Modified multiwall carbon nanotubes paste electrode as a sensor for simultaneous determination of 6-thioguanine and folic acid using ferrocenedicarboxylic acid as a mediator, J. Electroanal. Chem. 640 (2010) 75–83.
[20] D. Grieshaber, R. MacKenzie, J. Vörös, E. Reimhult, Electrochemical biosensors - sensor principles and architectures, Sens. (Basel, Switzerland) 8 (2008) 1400–1458.
[21] Q.M. Zhang, M.J. Serpe, Versatile method for coating surfaces with functional and responsive polymer-based films, ACS Appl. Mater. Interfaces 7 (2015) 27547–27553.
[22] C.M. Pandey, R. Singh, G. Sumana, M. Pandey, B. Malhotra, Electrochemical genosensor based on modified octadecanethiol self-assembled monolayer for Escherichia coli detection, Sens. Actuator B-Chem. 151 (2011) 333–340.
[23] T. Hosokai, A. Hinderhofer, F. Bussolotti, K. Yonezawa, C. Lorch, A. Vorobiev, Y. Hasegawa, Y. Yamada, Y. Kubozoro, A. Gerlach, S. Kera, F. Schreiber, N. Ueno, Thickness and substrate dependent thin film growth of picene and impact on the electronic structure, J. Phys. Chem. B 119 (2015) 29027–29037.
[24] A. Kaushik, P.K. Vabbina, V. Atluri, P. Shah, A. Vashist, R.D. Jayant, A. Yandart, M. Nair, Electrochemical monitoring-on-chip (E-MoC) of HIV-infection in presence of cocaine and therapeutics, Biosens. Bioelectron. 86 (2016) 426–431.
[25] M.A. Karymov, A.A. Kruchinin, Y.A. Tarantov, I.A. Balova, L.A. Remisova, N.G. Sukhodolov, A.I. Yanklovich, A.M. Yorkin, Langmuir-Blodgett film based membrane for DNA-probe biosensor, Sens. Actuator B-Chem. 6 (1992) 208–210.
[26] S.L. Selektor, M.A. Shcherbina, A.V. Bakirov, P. Batat, C. Grauby-Heywang, S. Grigorian, V.V. Arslanov, S.N. Chvalun, Cation-controlled Excimer packing in Langmuir–blodgett films of hemicyanine amphiphilic chromoionophores, Langmuir 32 (2016) 637–643.
[27] P.R. Solanki, A. Kaushik, V.V. Agrawal, B.D. Malhotra, Nanostructured metal oxide-based biosensors, NPG Asia Mater. 3 (2011) 17–24.
[28] Y.V. Stebunov, O.A. Aftenieva, A.V. Arsenin, V.S. Volkov, Highly sensitive and selective sensor Chips with graphene-oxide linking layer, ACS Appl. Mater. Interfaces 7 (2015) 21727–21734.
[29] A.F.D. Cruz, N. Norena, A. Kaushik, S. Bhansali, A low-cost miniaturized potentiostat for point-of-care diagnosis, Biosens. Bioelectron 62 (2014) 249–254.
[30] W. Zhong Lin, Zinc oxide nanostructures: growth, properties and applications, J. Phys. Condens. Matter 16 (2004) R829.
[31] S.S. Low, M.T.T. Tan, H.-S. Loh, P.S. Khiew, W.S. Chiu, Facile hydrothermal growth graphene/ZnO nanocomposite for development of enhanced biosensor, Anal. Chim. Acta 903 (2016) 131–141.
[32] S.K. Arya, S. Saha, J.E. Ramirez-Vick, V. Gupta, S. Bhansali, S.P. Singh, Recent advances in ZnO nanostructures and thin films for biosensor applications: Review, Anal. Chim. Acta 737 (2012) 1–21.
[33] E.A. Meulenkamp, Synthesis and growth of ZnO nanoparticles, J. Phys. Chem. B 102 (1998) 5566–5572.
[34] Y. Lv, L. Guo, H. Xu, L. Ding, C. Yang, J. Wang, W. Ge, S. Yang, Z. Wu, Low temperature synthesis and optical properties of small-diameter ZnO nanorods, J. Appl. Phys. 99 (2006) 114302.
[35] D. JapiÄ, I. Djerdj, M. MarinÅ¡ek, Z.C. Orel, In situ and ex situ TEOS coating of ZnO nanoparticles and the preparation of composite ZnO/PMMA for UV-VIS Absorbers, Acta Chim. Slov. 60 (2013) 797–808.
[36] B. Liu, H.C. Zeng, Hydrothermal synthesis of ZnO nanorods in the diameter regime of 50 nm, J. Am. Chem. Soc. 125 (2003) 4430–4431.
[37] K.D. Kim, D.W. Choi, Y.-H. Choa, H.T. Kim, Optimization of parameters for the synthesis of zinc oxide nanoparticles by Taguchi robust design method, Colloids Surf. A 311 (2007) 170–173.
[38] N.V. Konduru, K.M. Murdaugh, A. Swami, R.J. Jimenez, T.C. Donaghey, P. Demokritou, J.D. Brain, R.M. Molina, Surface modification of zinc oxide nanoparticles with amorphous silica alters their fate in the circulation,

Nanotoxicology (2015) 1–8.
[39] J. Tao, Z. Xiaofeng, Z. Jian, S. Yanling, L. Tianxing, A Zinc Oxide Modified Porous Silicon Humidity Sensor, Information Acquisition, 2006 IEEE International Conference on, 2006, pp. 1158–1162.
[40] H.-L. Xia, F.-Q. Tang, Surface synthesis of zinc oxide nanoparticles on silica Spheres: preparation and characterization, J. Phys. Chem. B 107 (2003) 9175–9178.
[41] G.A. Farzi, R. Tayebee, S. Naghibinasab, Surface modification of ZnO nanoparticles with Trimetoxyvinyl Silane and Oleic Acid and studying their dispersion in organic media, Int. J. Nano Dimens. 6 (2015) 67–75.
[42] C.M. Pandey, A. Sharma, G. Sumana, I. Tiwari, B.D. Malhotra, Cationic poly(lactic-co-glycolic acid) iron oxide microspheres for nucleic acid detection, Nanoscale 5 (2013) 3800–3807.
[43] Z. Matharu, G. Sumana, S.K. Arya, S.P. Singh, V. Gupta, B.D. Malhotra, Polyaniline Langmuir–Blodgett film based cholesterol biosensor, Langmuir 23 (2007) 13188–13192.
[44] M. Ramasamy, Y.J. Kim, H. Gao, D.K. Yi, J.H. An, Synthesis of silica coated zinc oxide–poly(ethylene-co-acrylic acid) matrix and its UV shielding evaluation, Mater. Res. Bull. 51 (2014) 85–91.
[45] Y. Xu, L. Axe, Synthesis and characterization of iron oxide-coated silica and its effect on metal adsorption, J. Colloid Interface Sci. 282 (2005) 11–19.
[46] C. Mouli Pandey, G. Sumana, I. Tiwari, Nanostructuring of hierarchical 3D cystine flowers for high-performance electrochemical immunosensor, Biosens. Bioelectron. 61 (2014) 328–335.
[47] S.K. Arya, T.S. Pui, C.C. Wong, S. Kumar, A.R.A. Rahman, Effects of the electrode size and modification protocol on a label-free electrochemical biosensor, Langmuir 29 (2013) 6770–6777.
[48] A. Sharma, C.M. Pandey, G. Sumana, U. Soni, S. Sapra, A. Srivastava, T. Chatterjee, B.D. Malhotra, Chitosan encapsulated quantum dots platform for leukemia detection, Biosens. Bioelectron. 38 (2012) 107–113.

Please cite this article in press as: C.M. Pandey, et al., Controlled deposition of functionalized silica coated zinc oxide nano-assemblies at the air/water interface for blood cancer detection, Analytica Chimica Acta (2016), http://dx.doi.org/10.1016/j.aca.2016.07.024